Energy Proceedings
Vol 51, 2025
ISSN 2004-2965

Numerical study of two-phase flow during evaporation in a microchannel coil evaporator for refrigeration systems

Xiaohui Yu*, Qinqin Kong, Sensen Jiang, Hongna Qiao

Hebei Key Laboratory of Thermal Science and Energy Clean Utilization, Hebei, School of Energy and Environment Engineering, Hebei University of Technology, Tianjin 300401, PR China

* Corresponding Author: 2018133@hebut.edu.cn

ABSTRACT

The miniaturization of electronic devices generates high heat flux, so evaporators that combine miniaturization and heat transfer capabilities are needed to meet the heat transfer requirements. In this paper, the inner flow and heat transfer characteristics of a microchannel coil evaporator were investigated using numerical analysis. The effects of evaporating pressure, and heat flux on the heat transfer coefficient, outlet temperature, and outlet vapor volume fraction were analyzed. In addition, a comparison was made with a rectangular evaporator designed with an equivalent diameter of 0.4 mm. The results indicate that the microchannel coil evaporator can reach the maximum outlet temperature of 53.75 °C, and the heat transfer coefficient is 1835.6 W/m^2. Compared to it, the area of the microchannel rectangular evaporator is reduced by 69% and the outlet temperature of the evaporator is decreased by 5.4% for the same amount of heat change. Meanwhile, the heat transfer coefficient has improved by 11.2%.

Keywords: numerical analysis, evaporating pressure, heat flux, microchannel coil evaporator, heat transfer coefficient

1. INTRODUCTION

The development of electronic devices tends to be highly integrated and miniaturization; this has led to a continuous increase in their heat flow density and an increase in their temperature [1]. It has been reported that a 10-20°C increase in the temperature of an electronic device doubles the probability of failure. If the temperature of an electronic device is lowered by 1°C, the failure rate is reduced by 4% [2]. Therefore, it is particularly important to reduce the temperature of electronic devices to keep them within a reasonable temperature range. At present, some heat dissipation methods (traditional air cooling, heat pipes, etc.) cannot meet the demand for efficient cooling of electronic devices, while microchannel gas-liquid two-phase heat transfer has the characteristics of compact size and high heat transfer capacity [3], which has been studied by many experts and scholars.

Luo et al [4] investigated the flow boiling heat transfer characteristics of R245fa in a horizontal smooth circular tube with an inner diameter of 10 mm and showed that the heat transfer coefficient decreases monotonically with the increase of vapor mass when the evaporation temperature reaches 105 °C. Chen et al [5] experimentally investigated the heat transfer mechanism, capacity, and flow characteristics of the boiling process in a pump-driven two-phase flow system commonly used in data center cooling, testing different coolants (R134a and R410a) and tube configurations (threaded and smooth). The heat transfer coefficients remained constant during saturated flow boiling due to the large variation in the mass flow rate of the coolant. Thiangtham et al [6] experimentally investigated the heat transfer characteristics of R134a in a microchannel heat sink. The heat transfer coefficients at heat flow densities of 40-120 kW/m^2, at high saturation temperatures (23 °C) were higher than those at low saturation temperatures (13 °C). Ricardo [7] investigated the flow boiling heat transfer of R134a in a smooth horizontal copper tube with an inner diameter of 13.84 mm and concluded that the heat transfer coefficients increased with the increase in mass velocity and heat flow densities at low gas volume fractions. Yan et al [8] conducted an experimental study of evaporative heat transfer for flow in a small horizontal circular pipe with an inner diameter of 2.0 mm. The heat transfer coefficients of the pipes proposed in this paper were 30-80% higher in most cases compared to the data reported in the literature for larger pipes (D>8.0 mm). Meng et al [9] investigated boiling two-phase flow within a vertically upward coiled U-bend with an inner diameter of 6 mm, where the phase transition in the U-bend transferred

This is a paper for the 16th International Conference on Applied Energy (ICAE2024), Sep. 1-5, 2024, Niigata, Japan.

more heat. The results showed that the performance of the U-tube heat exchanger with an elliptical cross-section was better than that of the heat exchanger with a circular cross-section. Dai et al [10] on the pipe diameter of 4, 6 mm smooth copper pipe for boiling heat transfer experimental study, the results show that the smaller the pipe diameter, the higher the saturation temperature, and the greater the boiling heat transfer coefficient.

In summary, most of the above studies conducted experimental or simulation studies on a single straight tube, and very few modeling studies were conducted on the whole coil. Therefore, in this paper, ANSYS FLUENT was used to model the whole microchannel coil channel with a three-dimensional gas-liquid two-phase evaporation process using a MIXTURE model in combination with the compiled evaporation condensation model UDF. Firstly, the flow heat transfer characteristics in the coil were analyzed, and secondly, the effects of inlet flow rate and evaporation pressure on its outlet, wall, and overall heat transfer characteristics were investigated. Since the microchannel coil evaporator is still large relative to the electronics, it is necessary to find an evaporator with a smaller size and larger heat transfer coefficient to meet the heat transfer demand. Considering the large pressure drop of the coil evaporator after size reduction, a final comparison with the rectangular microchannel evaporator was made to inform the next system design work.

2. MODEL BUILDING

2.1 Model building

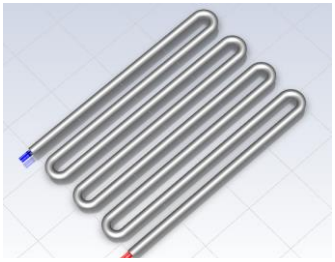

Fig. 1 Miniature coil evaporator model

The model is shown in Fig. 1, using a miniature coil evaporator model with an inner diameter of 6 mm and an outer diameter of 8 mm, with overall dimensions of 198 mm × 148 mm × 8 mm.

2.2 Modeling calculation

A UDF-compiled evaporation model was used to numerically simulate the flow and heat transfer in a microchannel coil evaporator.

The following assumptions were made for the model:

(1) the flow mass is an incompressible, continuous fluid;

(2) the radiative heat transfer in the evaporator is neglected;

(3) the sides and the top of the evaporator are adiabatic walls;

(4) the flow process is steady state. Considering the strong interphase interactions, a MIXTURE model is used to simulate the multiphase flow, which solves the equations of conservation of mass, momentum, and energy by the control volume method [11].

Continuity equation：

$$\nabla.(\rho_m \bar{V}_m) = 0$$

$$\bar{V}_m = \frac{\sum_{i=1}^{n} \alpha_i \rho_i \bar{V}_i}{\rho_m}$$

$$\rho_m = \sum_{i=1}^{n} \alpha_i \rho_i$$

Momentum equation：

$$\nabla.\left(\rho_m \bar{V}_m \bar{V}_m\right) = -\nabla P + \nabla.\left(\mu_m \nabla \bar{V}_m\right) + \nabla.\sum_{s=1}^{n}\left(\phi_x \rho_s \bar{V}_{d\tau,s} \bar{V}_{d\tau,x}\right) + \rho_m \bar{g}$$

Energy equation：

$$\nabla(\alpha_l \vec{v}_l(\rho_l E_l + p) + \alpha_v \vec{v}_v(\rho_v E_v + p)) = \nabla(k_{eff} \nabla T) + S_E$$

Velocity slip equation:

$$\vec{v}_{lv} = \frac{\tau_l}{f_{drag}} \frac{(\rho_l - \rho)}{\rho_l} \vec{a}$$

Second phase volume fraction equation：

$$\frac{\partial(\alpha_p \rho_p)}{\partial t} + \nabla\left(\alpha_p \rho_p \vec{v}_m\right) = -\nabla(\alpha_p \rho_p \vec{v}_{dr,p})$$

Phase transition equation：

The heat and mass transfer process occurs at the phase interface due to the absorption of heat by latent heat and transfer from the liquid phase to the gas phase. Using the Lee model and using self-written UDF, the liquid phase, gas phase mass transfer, and heat transfer source terms are added to the energy and continuity equations.

Importing them into the fluent model, the specific equations for the phase transition are as follows：

$$S_M = -\beta_e \alpha_l \alpha_l \frac{T - T_{sat}}{T_{sat}} \quad T > T_{sat}$$

Source terms of the energy equation：

$$S_E = h_{lv} S_M$$

2.3 Boundary conditions and solutions

To simulate the process of heating and evaporation, a uniform heat source is applied to the bottom half-wall surface of the evaporator, defining a constant heat flow density. The corresponding heat transfer coefficient is calculated as follows:

$$h_c = \frac{Q_c}{2\pi r L_c (T_b - T_e)}$$

The inlet is liquid and the velocity inlet is chosen as the boundary condition, the determination of which needs to be based on the Reynolds number Re, calculated as:

$$\mathrm{Re} = \frac{\rho \upsilon L}{\mu}$$

In the paper, the k-epsilon model is chosen for simulation and its turbulence intensity is calculated as follows:

$$I = 0.16(\mathrm{Re})^{-1/8}$$

The model treats R134a as a working fluid with a 100 percent fill rate of the evaporator section. In addition to liquid phase density and surface tension, the physical properties of the working fluid are assumed to be temperature-dependent to limit calculation time. These properties were obtained using the NIST REFPROP program [20] at (0.504-0.904 MPa). The evaporation process is imported using a compiled UDF, and the enhanced wall function is used to take the inlet flow rate (0.2-0.4 m/s), and the inlet temperature (294-304 K), which are by the operating conditions of a real miniature vapor compression refrigeration system. Considering that the outlet pressure and temperature are unknown, it is a free outflow.

In addition, a variety of pressure-velocity calculation methods are provided in Fluent, to reduce the calculation time and avoid convergence difficulties, the SIMPLEC algorithm is used, the second-order windward format is used for both momentum and energy; the residuals of both the continuity equation energy equation and momentum equation are less than 10^{-3}, the outlet temperature and the gas volume fraction of the gas are monitored, and convergence is considered to have been reached after all three have reached equilibrium.

2.4 Grid independence test

Divide the computational zone of the pipe into a finite control volume dominated by hexahedra. A boundary layer is used between the solid and fluid domains. To ensure the accuracy of the data, mesh-independent validation was performed for the model. In the same geometrical model, the temperature and gas volume fractions were compared for 100,300, 258,700, 592,800, 1,002,000, and 1,443,900 mesh numbers and the results are shown in Figure 2. As the number of grids increases, the change in temperature and gas volume fraction is less and hence the number of grids is chosen to be 592,800.

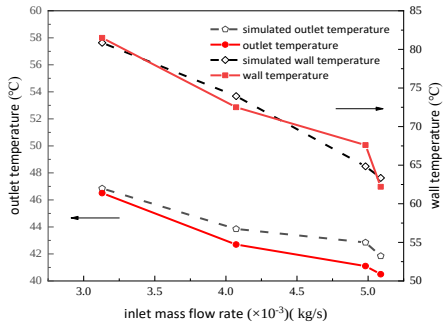

Fig.2 Effect of the number of grids on outlet temperature, wall temperature, and volume fraction of gas at the outlet of the evaporator

3. MODEL VALIDATION

To validate the numerical model of the evaporator, a vapor compression refrigeration system was built. Under the condition that the evaporator model is completely consistent, experiments and model validation are carried out.

The system includes a microchannel coil evaporator, a finned air-cooled condenser, an electronic expansion valve, and a micro DC compressor. The microchannel coil evaporator uses embedded electric heating with three heating tubes embedded in the bottom of the evaporator as the heat source of the evaporator; the condenser side is air-cooled. In this study, R134a is used as the refrigerant, and the vapor compression refrigeration system consists of four thermodynamic processes: evaporation and heat absorption into low-pressure and low-temperature gaseous vapor in the evaporator; adiabatic compression into superheated vapor in the compressor, followed by entering the condenser, cooling to saturated liquid at constant pressure, and then entering the evaporator cycle.

The parameters measured in the experiment include temperature, pressure, radiation intensity, and input power. The temperatures of the inlet and outlet of the evaporator and the wall temperature were measured at different compressor speeds and verified against the micro-coil evaporator model, and the results of the verification are shown in Fig. 3.

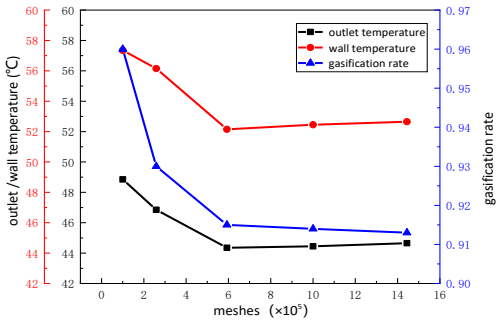

Fig.3 The validation of temperature

4. RESULTS AND DISCUSSION

4.1 Flow heat transfer characteristic

Temperature distribution, velocity distribution and gas volume distribution in a micro-coil evaporator all affect its flow heat transfer characteristics. The evaporation process of R134a in a microchannel coil evaporator was investigated under the working conditions of saturation pressure of P = 0.904 MPa, heat flow density q = 15000 W/m^2, and inlet flow rate of 0.3 m/s. Eight cross sections (L=0.16 m, L=0.32 m, L=0.64 m, L=0.80 m, L=1.12 m, L=1.28 m, L=1.60 m, L=1.76 m) with different positions from the pipe inlet were selected to investigate the temperature distribution, velocity distribution, and gas volume distribution.

Figure 4 shows the temperature distribution at different cross-sections. The overall average temperature shows an increasing trend with increasing tube length, while the temperature near the tube wall is higher concerning the whole fluid cross-section. This is because a constant heat flow density is applied to the lower half of the tube wall, the wall temperature increases, the fluid absorbs heat from the inlet, the heat gradually accumulates, and the temperature increases.

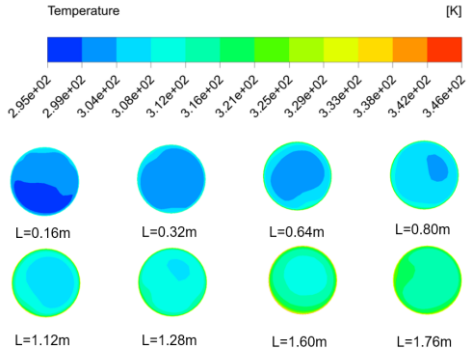

Fig.4 Temperature distribution of microchannel coil evaporator cross-section at different lengths from an inlet

Figure 5 represents the distribution of gas volume fraction at different cross sections. At the same cross-section, the gas volume is maximum around the pipe wall. As the distance from the inlet increases, the gas volume fraction is larger and the gas volume fraction is higher. Heating the pipe wall, the fluid R134a absorbs heat, reaches the evaporation temperature, and evaporates into a gas, at which time the density of the gas decreases, and at the same time is affected by the buoyancy force in the pipe cross-section against the upper position. Along the direction of the pipe length, the heat gradually accumulates, the liquid evaporation rate increases, and the gas volume fraction increases.

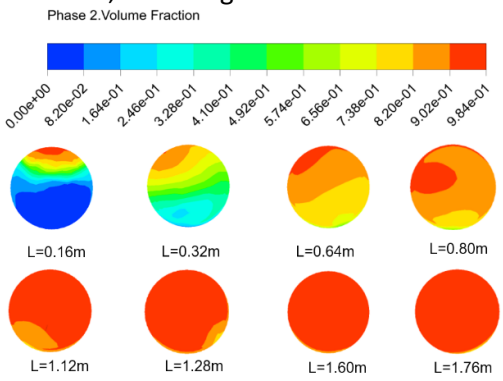

Fig.5 Volume fraction of vapor distribution of microchannel coil evaporator cross-section at different lengths from inlet

The distribution of the average velocity of the gas-liquid two-phase in the cross-section at different positions is shown in Fig. 6. From the figure, it can be observed that the average velocity of the gas-liquid two-phase is gradually increasing along the length of the pipe. The average velocity is larger above the cross-section of the pipe. This is because the gas is mainly distributed above; at a certain inlet flow rate (inlet is liquid), the gas density is less compared to the liquid density, so the velocity is greater. Along the direction of the pipe, the gas volume fraction increases, so the average velocity distribution of the gas and liquid phases increases.

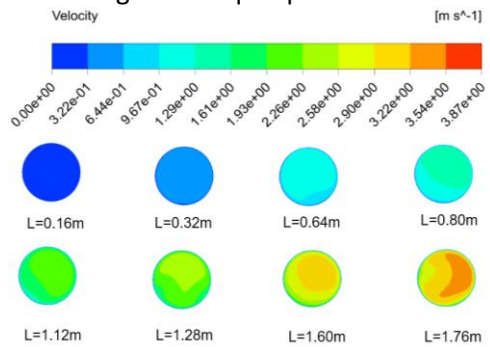

Fig.6 Average velocity distribution of microchannel coil evaporator cross-section at different lengths from the inlet

4.2 Inlet flow rate effects

Fig. 7 illustrates the variation of outlet temperature and wall temperature at saturation pressure of 0.904 MPa, inlet temperature of 294 K, and inlet flow rate of, 0.25, 0.3, 0.35, 0.4 m/s for different heat flow densities (15000, 12000, 9000 W/m^2).

As can be seen in Fig. 4, with the increase in inlet flow rate, the outlet temperature and wall temperature show an increasing trend. At a heat flow density of 15000 W/m^2, when the inlet flow rate increases from 0.2 m/s to 0.4 m/s, the outlet temperature decreases from 53.75 to 39.85 °C, a decrease of 25.9%; and the wall temperature decreases by 42.7%. At the same inlet flow rate, the higher the heat flow density, the higher the evaporator outlet temperature and wall temperature. However, as the inlet flow rate increases, the increase of the evaporator outlet temperature and wall temperature decreases. When the heat flow density decreases from 15,000 W/m^{2}to 9,000 W/m^{2}with an inlet flow rate of 0.2m/s, the outlet temperature decreases by 24.3% and the wall temperature decreases by 40.4%, while when the inlet flow rate is 0.4 m/s, the outlet temperature decreases by 6.0% and the wall temperature decreases by 21.1%.

The effect of the inlet flow rate on the wall temperature is greater than that of the outlet temperature. This is because the outlet temperature is more affected by the latent heat of gasification, and the increase in the heat transfer coefficient leads to a significant decrease in the wall temperature. Whereas, the higher velocity accelerates the flow and promotes the scouring of the liquid film, and the increase in the heat transfer coefficient leads to a smaller change in the outlet temperature.

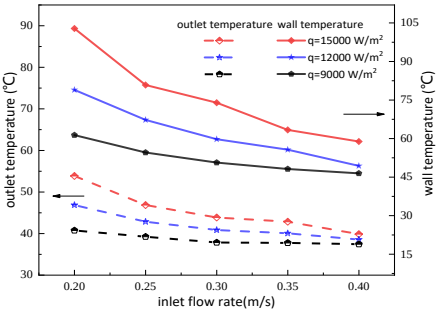

Fig.7 Impact of inlet velocity on outlet temperature and wall temperature of the evaporator

Fig. 8 represents the effect of the evaporator inlet flow rate on the outlet gas volume fraction. The greater the inlet velocity, the lower the gas volume fraction. This is because when the inlet velocity increases, the effect of gravity is weakened, which leads to the annular flow being more likely to occur when the overall heat transfer coefficient increases; the fluid flow is too fast, it is not easy to form a gasification core, which inhibits the nucleation of the boiling, so the gas volume fraction at the exit decreases, but the exit does not reach saturation due to the tube length is too short. In the heat flow density of 15000 W/m^2, the gas volume fraction decreases from 0.958 to 0.873 when the velocity increases from 0.2 m/s to 0.4 m/s. As the heat flow density increases, the gas volume fraction shows an increasing trend. When the velocity is certain, the gas volume fraction increases as the heat flow density increases. When the heat flow density increases from 9000 W/m^2 to 15000 W/m^2, the gas volume fraction increases from 0.776 to 0.873 This is because the increase in heat flow density leads to a larger temperature difference between the fluid and the wall, which strengthens the nucleation boiling and facilitates the formation of the gasification core.

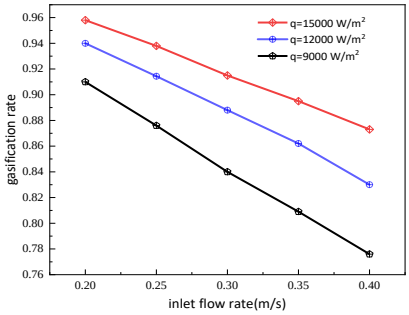

Fig.8 Impact of inlet velocity on volume fraction of vapor

Fig. 9 represents the effect of the evaporator inlet flow rate on the heat transfer coefficient. As the inlet flow rate increases, the heat transfer coefficient increases. When the heat flow density is 9000 W/m^2, the inlet velocity increases from 0.2 m/s to 0.4 m/s, and the growth rate of the heat transfer coefficient is 27.2%, while the growth rate is 20.8% when the heat flow density is 15000 W/m^2.This is due to the evaporator inlet flow rate being larger, the higher the heat flow density, the higher the frequency of bubble departure, and the ring flow is more likely to form, so by strengthening the nuclear state boiling, the heat transfer coefficient increases.

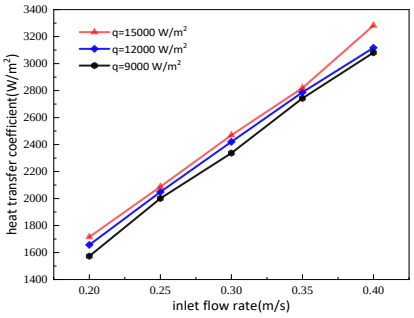

Fig.9 Impact of inlet velocity on the volume fraction of heat transfer coefficient

5. CONCLUSIONS

In this paper, a three-dimensional microchannel coil evaporator was built by combining the MIXTURE, velocity slip model, and finite element method to simulate the evaporation process of its gas-liquid two-phase. In addition, the effect of the inlet flow rate is analyzed and some conclusions are drawn as follows:

1. For the same cross-section, the temperature, gas volume, and velocity have larger values around the pipe wall. The further away from the inlet position, the greater the average cross-section temperature, gas volume fraction, and velocity.

2. As the inlet flow rate increases, the heat transfer coefficient increases; while the evaporator outlet temperature and gas volume fraction of the gas decrease. Heat flow density of 15000 W/m^2, inlet flow rate from 0.2 m/s increased to 0.4 m/s, the heat transfer coefficient from 1835.6 W/m^2 to 3333.6 W/m^2; outlet temperature from 53.75 °C to 39.85°C; gas volume fraction from 0.958 to 0.873.

ACKNOWLEDGEMENT

This study was supported by the National Key R&D Program of China (No. 2022YFE0208300) and a grant from the Central Guiding Funds for Local Science and Technology Development Projects (No. 236Z4503G) and a grant from the Industry-University-Research Collaboration Projects of Shijiazhuang in Hebei Province (No. 241010071A).

REFERENCE

[1] ZAHID I, FARHAN M, FAROOQ M, et al. Experimental investigation for thermal performance enhancement of various heat sinks using Al2O3 NePCM for cooling of electronic devices [J]. Case Studies in Thermal Engineering, 2023, 41: 102553.

[2] REZK K, ABDELRA HMAN M A, ATTIA A A A, et al. Thermal control of temperature-sensitive electronic components using a vapor chamber integrated with a straight fins heat sink: An experimental investigation [J]. Appl Therm Eng, 2022, 217: 119147.

[3] FANG L,ZHIPENG Y,WEIXING Y, et al. Experimental research on the convective heat transfer and pressure drop of forced-flow boiling in micro-channels heat exchanger [J]. Journal of Engineering Thermophysics, 2023, 44(08): 2240-9.

[4] Luo X, Xia Y, Huang J, et al. Experimental investigation on high-temperature flow boiling heat transfer characteristics of R245fa in a horizontal circular tube[J]. Applied Thermal Engineering, 2023, 225: 120260.

[5] CHEN X, DING T, CAO H, et al. Flow boiling heat transfer mechanisms and flow characteristics of pump-driven two-phase flow systems used in data center cooling [J]. Appl Therm Eng, 2023, 220: 119642.

[6] THIANGTHAM P, KEEPAIBOON C, KIATPACHAI P, et al. An experimental study on two-phase flow patterns and heat transfer characteristics during boiling of R134a flowing through a multi-microchannel heat sink [J]. International Journal of Heat and Mass Transfer, 2016, 98: 390-400.

[7] DA SILVA LIMA R J, QUIBéN J M, THOME J R. Flow boiling in horizontal smooth tubes: New heat transfer results for R-134a at three saturation temperatures [J]. Appl Therm Eng, 2009, 29(7): 1289-98.

[8] YAN Y-Y, LIN T-F. Evaporation heat transfer and pressure drop of refrigerant R-134a in a small pipe [J]. International Journal of Heat and Mass Transfer, 1998, 41(24): 4183-94.

[9] Meng M, Peng X F. Influence of U-bend heterogeneous effects on bubble dynamics and local flow boiling heat transfer in hairpin tubes[J]. International Journal of Thermal Sciences, 2011, 50(10): 2016-2026.

[10] YUNADE D,QINHAN L,SIKAI Z, et al. Boiling heat transfer performances of R290 in smooth horizontal tubes [J]. CIESC Journal, 2017, 68(09): 3420-6.

[11] TIANZI F,Numerical study on boiling heat transfer in horizontal tube with small diameter [D]; Huazhong University of Science and Technology, 2022.